Crystal Structures and Magnetic Properties of a Set of Uncommon Dihalo-Bridged Oxalamidato Copper(II) Dimers

Žilić, Dijana; Rakvin, Boris; Milić, Dalibor; Pajić, Damir; Đilović, Ivica; Cametti, Massimo; Džolić, Zoran

Permanent link / Trajna poveznica: https://urn.nsk.hr/urn:nbn:hr:217:869194

Download date / Datum preuzimanja: **2024-06-30**

Repository / Repozitorij:

Repository of the Faculty of Science - University of Zagreb

Crystal Structures and Magnetic Properties of a Set of Uncommon Dihalo-Bridged Oxalamidato Copper(II) Dimers†

Dijana Žilić,[a] Boris Rakvin,[a] Dalibor Milić,[b‡] Damir Pajić,[c] Ivica Đilović,[b] Massimo Cametti[d] and Zoran Džolić*[a]

A set of four copper(II) complexes, L^1–X and L^2–X (X = Cl, Br; L^1 = *N*-(L-leucine methyl ester)-*N*'-((2-pyridin-2-yl)methyl)oxalamide and L^2 = *N*-benzyl-*N*'-((2-pyridin-2-yl)methyl)oxalamide) have been synthesized and characterized by X-ray structural analysis, electron paramagnetic resonance (EPR) spectroscopy on single crystal and by SQUID magnetization measurements. X-ray diffraction studies show one-dimensional hydrogen bonded networks of dimeric copper(II)-complexes bridged by two halide ions and with the two metal centers 3.44–3.69 Å apart. The geometry at each copper(II) atom is ideal or near ideal square pyramidal. ESR and SQUID studies indicate that all complexes exhibit weak antiferromagnetic interactions between the Cu(II) paramagnetic centers, with exchange parameter $|J| \sim 1$ cm^{-1}. Magneto-structural comparisons among similar dihalo-bridged Cu(II) binuclear complexes are also provided, and a possible correlation has been established.

1 Introduction

Dinuclear copper(II) complexes have aroused considerable interest over the last few decades, not only for the role played in catalytic enzymatic reactions,[1] but also because they possess essential structural features for the study of magnetic interactions between two close magnetic centers.[2,3] Not surprisingly, the different chemical environment around the copper ions may greatly influence the resulting magnetic behavior. Hence, the investigation of the magnetic properties of such complexes in light of their relation to structural features are often attempted seeking the discovery of definite magneto-structural relationships whose utility increases more, the larger their field of applicability is. In general, correlations of this kind are not easily obtained, especially due to a large structural variability. Taking into consideration a smaller ensemble of Cu(II) complexes, for example, the dihalo-bridged Cu(II) complexes,[4,5] the situation improves a little. However, the structural variability remains wide. Indeed, the metal centers can be four- or five-coordinated, depending on the nature of the ligands, and this gives rise to a variety of different structures, ranging from square-pyramid to trigonal bipyramid.[6]

Over the years, several theoretical analyzes have been carried out to obtain an empirical relationship between an exchange coupling constant and structural features for copper(II) complexes and to explain different magnetic behaviors, from ferro- to antiferromagnetic interactions.[7] Magneto-structural correlation in dihalo-bridged copper(II) complexes seems to be more complicated compared to dihydroxo-bridged complexes.[8–10] It should be noted also, that among dihalo-bridged complexes, the vast majority of reports are related to dichloro species and considerably less information is available on structural and magnetic properties of dibromo-bridged copper(II) dimers.[10,11]

N,*N*'-disubstituted oxalamides have proved to be very useful ligands in designing homo- and heterometallic complexes.[12] Indeed, they provide a tunable molecular environment due to *cis-trans* conformational freedom, different coordination geometries and ligand charges availability (for example by NH deprotonation). On the other hand, the studies on the metal complexes involving oxalyl retro-peptide ligands are very limited. Given the interesting properties that the above mentioned ligands might bring about, we have designed and synthesized four dihalo-bridged copper(II) oxalamidato dimers: [CuL^1(μ-Cl)]$_2$·CH$_3$OH (L^1–Cl), [CuL^2(μ-Cl)]$_2$ (L^2–Cl), [CuL^1(μ-Br)]$_2$ (L^1–Br) and [CuL^2(μ-Br)]$_2$ (L^2–Br), where ligands L^1 and L^2 stand for *N*-(L-leucine methyl ester)-*N*'-((2-pyridin-2-yl)methyl)oxalamide and *N*-benzyl-*N*'-((2-
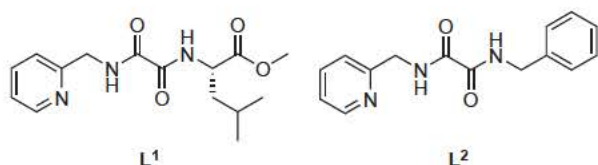
Fig. 1 Schematic presentation of ligands N-(L-leucine methyl ester)-N'-((2-pyridin-2-yl)methyl)oxalamide (L^1) and N-benzyl-N'-((2-pyridin-2-yl)methyl)oxalamide (L^2).

pyridin-2-yl)methyl)oxalamide, respectively (Figure 1).

To the best of our knowledge, the described compounds represent the first set of structures of oxalamido-complexes which display discrete dinuclear dihalo-bridged units.

The magnetic characterization of the compounds was performed by Electron Paramagnetic Resonance (EPR) spectroscopy and SQUID magnetization measurements. Single crystal EPR spectroscopy performed on the dinuclear copper complexes provided information about the coordination geometry around copper(II) ions. Moreover, from the angular dependence of linewidth, additional information about the mechanism of interaction between copper(II) ions were obtained. Temperature and field dependencies of magnetization was used for determination isotropic exchange interaction between copper ions. Finally, a relation between magnetic behavior and molecular structure of the investigated complexes have been presented and discussed in the frame of existing correlations for dihalo-bridged copper(II) complexes.

2 Material and methods

The preparations and structural details of ligands L^1 and L^2 have been previously described.[13] Complexes L^1–Cl, L^2–Cl, L^1–Br and L^2–Br were prepared by the reaction of equimolar quantities of ligands with $CuCl_2 \cdot 2H_2O$ or $CuBr_2$ in methanol. Single crystals suitable for X-ray diffraction were obtained by slow evaporation of corresponding methanol solutions.

2.1 X-ray crystallographic study

We have already reported single-crystal X-ray structural analysis of L^1–Cl (CCDC 907166).[13] X-ray difraction data from single crystals of L^2–Cl, L^1–Br and L^2–Br were collected on an Oxford Diffraction Xcalibur 3 CCD diffractometer with graphite-monochromated $MoK\alpha$ radiation ($\lambda = 0.71073$ Å) and reduced using the CrysAlis PRO software package.[14] The solution (SHELXS),[15] refinement (SHELXL-97),[15] building and analysis of the structures were performed using Coot[16] and the programs integrated in the WinGX system[17]. Data processing and refinement statistics are given in Table 1. All non-hydrogen atoms were refined anisotropically. H atoms

attached to C atoms were positioned geometrically and refined isotropically applying the usual riding model [d(C–H) $= 0.93$–1.00 Å and U_{iso}(H) $= 1.2$ or $1.5U_{eq}$(C)]. H atom attached to N3 in L^2–Cl was refined isotropically with a restraint on the N–H distance (DFIX 0.86 0.02), while H atoms of the same type in L^1–Br and L^2–Br were positioned geometrically and refined by using the appropriate riding model [AFIX 43, d(N–H) $= 0.88$ Å and U_{iso}(H) $= 1.2U_{eq}$(N)]. N-benzyl moiety in L^2–Cl is discretely disordered over two conformations with the relative population parameter 0.840(5) for the major one. The disordered atoms in L^2–Cl were refined with restraints on their geometrical (SAME) and displacement parameters (SIMU, DELU, ISOR). The final structural models were analyzed using PLATON.[18] Molecular graphics were prepared in Mercury,[19] ORTEP-3,[20] and POV-Ray.[21]

2.2 EPR study

EPR measurements were performed on the single crystals and on the powder forms of the investigated compounds. EPR experiments were carried out with a Bruker 580 FT/CW X-band spectrometer equipped with a standard Oxford Instruments model DTC2 temperature controller. The microwave frequency was ≈ 9.6 GHz with the magnetic field modulation amplitude of 0.5 mT at 100 kHz. The crystals of chloride (bromide) compounds were elongated along the crystallographic b (a)-axis. They were rotated round three mutually orthogonal axes: a crystallographic b (a)-axis, an arbitrary chosen c^* (b^*)-axis perpendicular to b (a)-axis and a third a^* (c^*)-axis, perpendicular to the previous two axes. EPR spectra were recorded at 5° steps and the rotation was controlled by a home-made goniometer with the accuracy of 1°. A larger uncertainty (2–3°) was related to the optimal deposition of the crystals on the quartz holder. The EPR spectra were measured at two temperatures: $T = 297$ K and $T = 80$ K.

2.3 Magnetization study

Magnetic measurements of the investigated compounds in form of powders were performed using commercial MPMS5 SQUID magnetometer. Temperature dependent magnetization $M(T)$ for 2 K $< T <$ 300 K was measured in constant magnetic field of 1000 Oe and after correction against the sample holder, the temperature independent contributions of inner electrons were also subtracted. Field dependence of magnetization $M(H)$ was measured at lowest temperature of 2 K in field up to 5 T.

Table 1 X-ray crystallographic data for **L²–Cl**, **L¹–Br** and **L²–Br**

Structure	L²–Cl	L¹–Br	L²–Br
Chemical formula	$C_{30}H_{28}Cl_2Cu_2N_6O_4$	$C_{30}H_{40}Br_2Cu_2N_6O_8$	$C_{30}H_{28}Br_2Cu_2N_6O_4$
M_r	734.56	899.58	823.48
Crystal color, habit	Blue, plate	Blue, prism	Blue-green, plate
Crystal size (mm^3)	0.01 x 0.20 x 0.75	0.15 x 0.40 x 0.50	0.05 x 0.10 x 0.10
Crystal system	Monoclinic	Triclinic	Triclinic
Space group	$P2_1/c$	$P1$	$P\bar{1}$
a (Å)	7.7369(3)	8.4814(3)	8.0988(6)
b (Å)	9.8930(3)	9.3314(4)	9.6585(6)
c (Å)	21.9325(10)	11.7613(3)	10.1449(6)
α (°)	90	81.072(3)	93.172(5)
β (°)	101.955(4)	78.321(3)	90.749(5)
γ (°)	90	76.097(4)	94.721(5)
V (Å³)	1642.33(11)	879.28(6)	789.53(9)
Z	2	1	1
T / K	150(1)	150(1)	120(1)
D_{calc} (g cm⁻³)	1.485	1.699	1.732
μ (mm⁻¹)	1.501	3.538	3.923
Data total/unique	10974/3231	9239/6032	9243/2771
R_{int}	0.042	0.014	0.084
Observed data [$I > 2\sigma(I)$]	2607	5715	1927
Restraints/parameters	185/258	3/433	0/199
$R_1[I > \sigma(I)]$	0.0366	0.0196	0.0465
wR_2 (all data)	0.0891	0.0508	0.0902
S	1.04	1.04	0.99
Flack parameter	n/a	0.015(7)	n/a
Min. and max. resd. dens. (e Å⁻³)	−0.57, 0.51	−0.36, 0.32	−0.50, 0.83
CCDC number	919441	919442	919443

3 Results and discussion

3.1 Description of structures

Oxalyl retro-peptides compounds represent a versatile class of molecules which has been previously employed, with considerable success, in the study of gel formation.[22] There are only few examples of structurally characterized halo-bridged oxalamidato metal complexes.[23–25] Mixing equimolecular amounts of $CuCl_2 \cdot 2H_2O$ or $CuBr_2$ and the asymmetrical N,N'-disubstituted oxalamide ligands L^1 and L^2 in MeOH did not result in oxalamidato-bridged complexes, as in the cases of copper(II) nitrate or perchlorate and the symmetrical N,N'-bis-(2-methylpyridyl)-oxalamide.[26] Instead, the dihalo-bridged dinuclear complexes L^1– and L^2–X (X = Cl and Br) were obtained (Figure 2).

In all cases, the X-ray determined structures of the complexes show penta-coordinated Cu(II) ions adopting a square pyramidal geometry. The square base coordination sites are occupied by a deprotonated ligand, acting as NNO tridentate, and by one of the bridging halo-ions; the apical position of the pyramid is instead occupied by the other bridging halo-ion, as shown in Figure 3. The coordination polyhedron around the copper(II) ion could be best described as an ideal or near ideal square pyramid, with $\tau = 0.00$–0.17 (where $\tau = 0$ implies the ideal square-pyramidal geometry and $\tau = 1$ an ideal trigonal bipyramid;[27] Table 2). As said, the two Cu(II) centers are bridged by two halo-ions in such a way that the two square pyramids share one base-to-apex edge while having their basal planes parallel (Figure 3). Rodríguez et al. have designated this kind of configurations for copper complex containing the $Cu–(\mu–X)_2–Cu$ core as a type II pyramidal arrangement.[28] Although the dimeric molecules with achiral ligand L^2 are positioned on the crystallographic inversion centers, N-benzyl groups in L^2–Cl are discretely disordered over two conformations (Figure 2).

Bond distances and angles relevant to the coordination of copper(II) ions are given in Table 2. The Cu_2X_2 unit is planar in all the four dimers with the bridging Cu–X–Cu' angles [86.53(3)–91.50(3)°] being close to a right angle and the Cu$\cdots$Cu' intra-dimeric distances ranging from 3.4408(4) to 3.6852(6) Å. As similarly as in other dihalo-bridged Cu(II) complexes with square-pyramidal coordination,[29,30] the axial Cu–X bonds [2.6674(8)–2.7582(6) Å in the Cl-complexes, 2.7475(9)–2.8282(5) Å in the Br-complexes] are significantly longer than the corresponding basal Cu–X bonds [2.2221(6)–2.2443(8) Å in the Cl-complexes, 2.3910(5)–2.4056(9) Å in the Br-complexes], due to Jahn-Teller effect. However, the coordination to a negatively charge ligand (at the oxalamidato N atoms N2 or N5), shortens the observed Cu–N(oxalamide) bonds in all complexes [1.896(4)–1.917(4) Å] with respect to usual Cu–N(pyridyl) bonds [1.996(4)–2.034(4) Å], observed
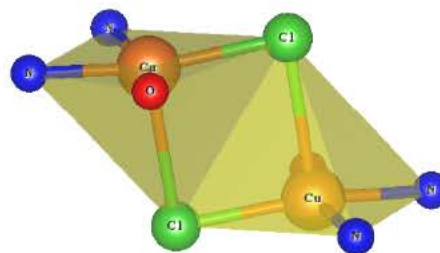

Fig. 3 For the all investigated compounds, the coordination environment around Cu(II) is an ideal or near ideal square-pyramidal. Cu(II) ions are penta-coordinated by an oxalamidato O and N, pyridyl N atom and two halo-ions (X^-; X = Cl or Br). The halo-ion that is farther from the Cu(II) occupies the apical position of the square pyramid. Two pyramids share one base-to-apex edge with parallel basal plane.

in similar copper(II) complexes, for example those made of N,N'-bis-(2-methylpyridyl)-oxalamide.[26]

Within the crystal, in all cases, the complexes are linked to each other by hydrogen bonds between oxalamide units (Figure 4; Table 5 in the Supporting Information, SI) and form infinite chains of dinuclear units. Such supramolecular arrangement resembles the structure of the only linear-chain Cu(II) compound reported so far which displays alternating dichloro- and oxalamidato-bridges.[23] Stacking interactions between pyridyl and metalloaromatic chelate ring[31] (Cu–O–C–C–N in our case), which we have observed for L^1–Cl,[13] are also present in crystal structures of the bromo-complexes (Table 6 and Figures 10 and 11 in SI), but - surprisingly - not in L^2–Cl. In addition, we also found weak hydrogen bonds C–H$\cdots A$ and C–H$\cdots\pi$ interactions with either a chelate[32] or a phenyl ring (as detailed in Tables 5 and 7 in SI). Intriguingly, the crystal packing of L^2–Cl molecules allows discrete conformational disorder of their N-benzyl groups (Figure 10 in SI), while preserving C–H$\cdots\pi$ interactions for both observed conformations (Table 7 in SI). An aryl π–π stacking interaction exists only between two phenyl rings in the crystal structure of L^2–Br (Figure 12 and Table 6 in SI).

3.2 EPR study

The single crystal EPR spectrum of complex L^1–Cl shows single, fairly Lorentzian, line in every direction of the magnetic field. Similar spectra are observed also for the dibromo-bridged complexes L^1–Br and L^2–Br. Differently, the complex L^2–Cl shows a single line in only one rotation plane and double lines in other two (except for directions close to the crystal axes). The observed number of EPR lines can be simply correlated to the number of molecules (dimers), Z, found in the unit cell. In the L^1–Cl, L^1–Br and L^2–Br complexes Z = 1, while Z = 2 for L^2–Cl complex. Moreover,
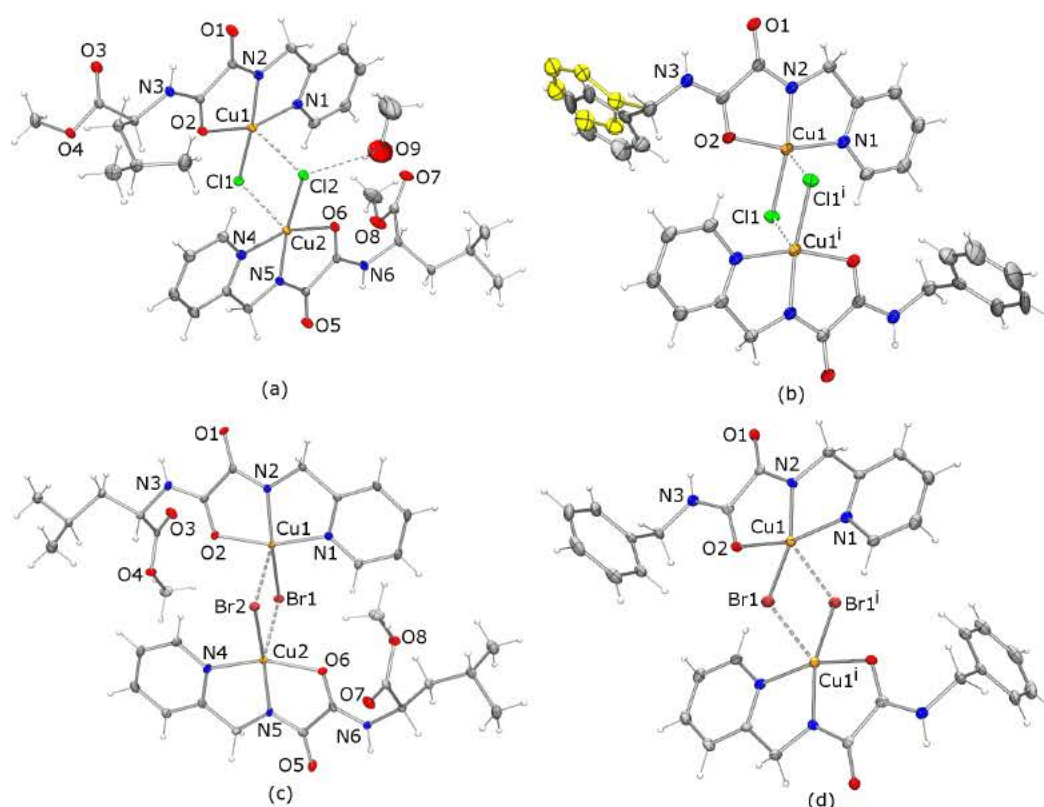
Fig. 2 The molecular structures of complexes (a) **L^1–Cl**, (b) **L^2–Cl**, (c) **L^1–Br** and (d) **L^2–Br**. Displacement ellipsoids are drawn at the 30% probability level. H atoms are shown as spheres of an arbitrary radius. Dashed lines represent the O–H⋯Cl hydrogen bond in **L^1–Cl** and the apical Cu–X bonds (X = Cl or Br) in all the complexes. Atoms labeled with "i" in **L^2–Cl** and **L^2–Br** are centro symmetrically related to those in the other half of a molecule. The less populated conformation [the relative population parameter 0.160(5)] of the disordered *N*-benzyl group in **L^2–Cl** (yellow) is shown only for a crystallographically independent half of the dinuclear complex. Although modeled, H atoms in this conformation are not depicted for clarity.

Table 2 Molecular geometry (Å, °, °/Å) of the analyzed complexes

	L^1–Cl^{a} [13]		L^2–Cl	L^1–Br^{a}		L^2–Br
Cu–X^{b} (basal)	2.2221(6)	2.2552(6)	2.2443(8)	2.4001(5)	2.3910(5)	2.4056(9)
Cu–X (axial) (*R*)	2.7582(6)	2.7049(6)	2.6674(8)	2.8282(5)	2.8071(5)	2.7475(9)
Cu–O (oxalamide)	2.064(2)	2.052(2)	2.010(2)	2.013(3)	2.055(3)	2.026(3)
Cu–N (pyridyl)	2.030(2)	2.014(2)	2.003(2)	1.996(4)	2.034(4)	2.007(4)
Cu–N (oxalamide)	1.899(2)	1.906(2)	1.910(2)	1.917(4)	1.910(4)	1.896(4)
τ^{c}	0.17	0.15	0.02	0.04	0.00	0.10
d(Cu)^{d}	0.1310(2)	0.1828(2)	0.1990(3)	0.2282(4)	0.2362(5)	0.2492(7)
Cu⋯Cu'	3.5239(3)		3.4408(4)	3.6852(6)		3.5405(9)
Cu–X–Cu' (α)	90.78(2)	88.73(2)	91.50(3)	89.74(2)	89.43(2)	86.53(3)
α/R	32.91	32.80	34.30	31.73	31.86	31.49

^{a} Data are given for each of the two crystallographically independent parts of a dinuclear complex.
^{b} X = Cl or Br.
^{c} Reedijk's trigonal distortion τ (ideally, $\tau = 0$ for a square-pyramidal and $\tau = 1$ for a trigonal-bipyramidal geometry). [13]
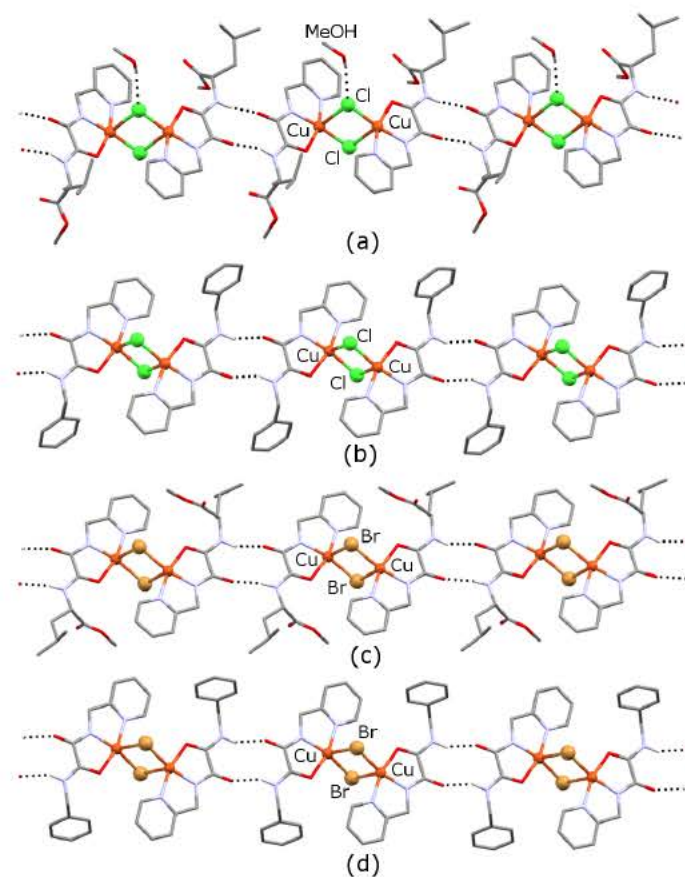^{d} Displacement of Cu atom from the mean basal plane.

Fig. 4 Infinite molecular chains in the crystal structures of (a) L^1–Cl, (b) L^2–Cl, (c) L^1–Br and (d) L^2–Br formed by hydrogen-bonding (dotted lines) between oxalamide units. The minor conformation of the disordered *N*-benzyl moiety in L^2–Cl and the H atoms attached to C atoms are omitted for clarity.

while dimeric units for L^{2-} complexes are crystallographically centrosymmetric and, thus, the two bridged copper centers are magnetically equivalent, different is the case for L^{1-} complexes whose dimeric units are constituted by magnetically nonequivalent copper ions. Hence, the observation of one line - instead of two lines - in the EPR spectra of these latter compounds points to an existence of exchange interaction with $2J > \Delta g \beta H$, where Δg is the difference between g-factors of the copper ions and other symbols have their usual meaning.[33] Hyperfine interactions or any half-field transitions associated with a $\Delta M_s = \pm 2$ were not detected from room temperature down to 80 K.

Angular dependencies of g-factor and peak-to-peak linewidths, W_{pp}, recorded at room temperature, are presented in Figure 5, as well as in Figures 13–15 in SI. The dependencies obtained at $T = 80$ K were approximately the same as those at room temperature and therefore, they are omitted.

The elements of a $(\mathbf{g^T g})$-tensor were determined using the following equation[34]:

$$
\begin{aligned}
g^2 = \quad & (\mathbf{g^T g})_{aa} \sin^2\theta \cos^2\phi + (\mathbf{g^T g})_{ab} \sin^2\theta \sin 2\phi + \\
& + (\mathbf{g^T g})_{bb} \sin^2\theta \sin^2\phi + (\mathbf{g^T g})_{ac} \sin 2\theta \cos\phi + \\
& + (\mathbf{g^T g})_{bc} \sin 2\theta \sin\phi + (\mathbf{g^T g})_{cc} \cos^2\theta \qquad (1)
\end{aligned}
$$

where θ and ϕ are the polar and azimuthal angles of the magnetic field vector $\mathbf{B}$ in the a^*–b–c^* (a–b^*–c^*) coordinate system, respectively. The calculated g-tensors are presented in Figure 5 and in Figures 13–14 in SI. Some EPR lines for the compound L^2–Br were too weak and/or to broad to be detected, therefore the calculation of g-tensor for this complex was not performed. The principal values of the g-tensors, obtained by diagonalization of the $\mathbf{g^T g}$-matrix at room temperature, are shown in Table 3, with the estimated error ± 0.0001. Powder averaged values g_{av} are calculated as: $g_{av} = \sqrt{(1/3)(g_x^2 + g_y^2 + g_z^2)}$. The principal axis g_z is directed along Cu–X bond (X ion at apical position), while g_x and g_y lay in the basal plane of square pyramid. The obtained $g_z > g_x, g_y$ values point out that the $d_{x^2-y^2}$ is the highest energy half-occupied orbital[35], that is in agreement with the square-pyramidal coordination around Cu(II) ions, as could be seen from Table 2.

The powder EPR spectra of the investigated compounds recorded at $T = 297$ K and $T = 80$ K are shown in Figure 6. The spectra can be simulated using only g-tensors parameters obtained from the single crystal measurements given in Table 3 while hyperfine A-tensors were taken to be zero. The powder spectra for complex L^2–Br are simulated assuming the following parameters: $g_x = g_y = 2.13$ and $g_z = 2.39$. The spectra were simulated by *EasySpin* software[36] using Lorentzian lineshapes, with only different linewidths at different temperatures.
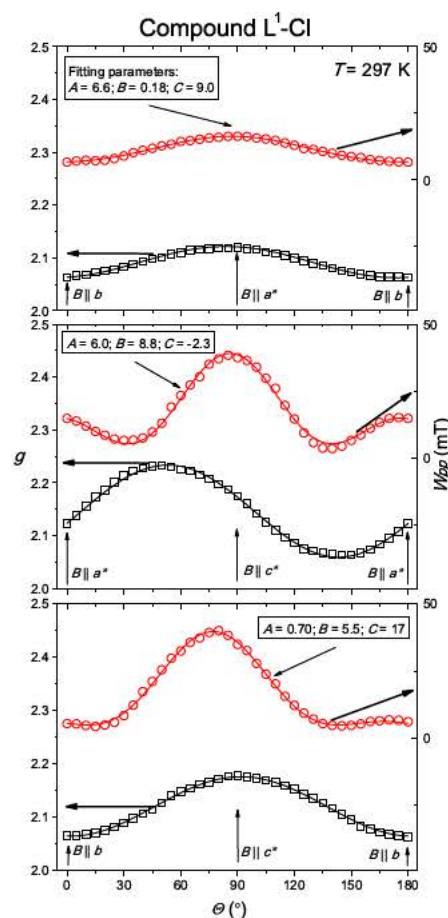
Fig. 5 Angular variation of the g-values (black squares) and the W_{pp} linewidths (red circles) of EPR lines for the single crystal of compound L^1–Cl, at room temperature, in three mutually perpendicular planes. Solid lines represent the fitted g-values with parameters given in Table 2 and W_{pp} linewidths with parameters given in the figure, according to eq 1 and eq 2, respectively.

Table 3 Principal and average values of the g-tensors of the analyzed compounds at room temperature

Compounds	g_x	g_y	g_z	g_{av}
L^1–Cl	2.0559	2.0662	2.2335	2.1201
L^2–Cl	2.0504	2.0628	2.2352	2.1178
L^1–Br	2.0459	2.0847	2.2525	2.1296
L^2–Br	–	–	–	–

Fig. 6 Experimental (solid lines) and simulated (dotted lines) X-band EPR spectra of powdered samples of the compounds at the indicated temperatures.

The observed EPR linewidth data show strong angular dependence, as could be seen in Figure 5 and in Figures 13–15 in SI. Linewidth minima are observed for some angles θ between $0°$ and $90°$. A similar linewidth anisotropy has been observed for layered compounds. This behavior is in contrast to the 3D situat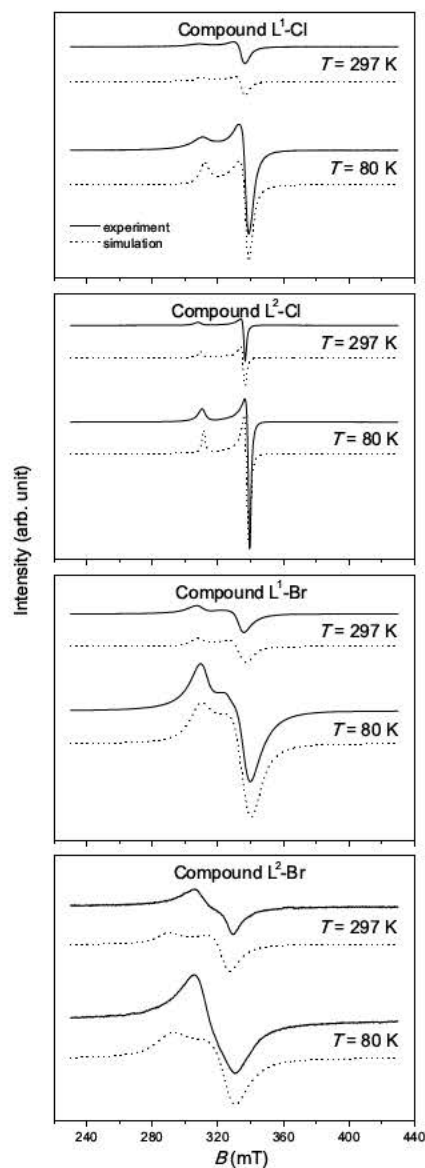ion, where the linewidths show dependence $(1 + \cos^2 \theta)$. The minimum lays close to the magic angle $\theta = 55°$ is characteristic for low-dimensional systems and it corresponds to the secular part of the dipolar interaction $(3 \cos^2 \theta - 1)^2$.[37] However, this term was not enough to explain observed linewidth data and we have considered additional sources of EPR line broadening and narrowing. The data were fitted adequately, presented by solid lines in Figure 5 and Figures 13–14 in SI by using the general expression:[38]

$$\Delta W_{pp} = A + B(3 \cos^2 \theta - 1)^2 + C \cos^2 \theta. \quad (2)$$

The A-term represents the isotropic contribution to the linewidth, the B-term describes the previously mentioned dipolar interaction, while the C-term could be related to anisotropic spin-spin interaction. The values of the parameters A, B and C are given in Figure 5 and in Figures 13–14 in SI. Hyperfine term and contribution arising on the non-equivalence of the copper sites for compounds $\mathbf{L^1}$–**Cl** and $\mathbf{L^1}$–**Br** were neglected in eq 2.

The obtained results, the absence of hyperfine interactions (with the copper as well as two nitrogen nuclei), the unifying line effect for magnetically non-equivalent copper centers and Lorentzian-like EPR lines, reveal the presence of an exchange interaction in the compounds. However, the absence of half-field EPR line shows that this interaction is not strong. By using linewidth analysis and method of moments[39]:

$$\Gamma_{exp} \sim \gamma (\Gamma_d)^2 / \omega_{exch} \quad (3)$$

where Γ_{exp} is the experimental linewidth, γ is the gyromagnetic ratio, $\omega_{exch} \sim J\sqrt{S(S+1)}$ and Γ_d is the dipolar linewidth due to the contribution of the nearest copper ions ($\Gamma_d \sim B$ from eq 2), calculated as previously described,[40] an exchange interaction parameter between copper(II) ions in the order of $|J| \sim 1$ cm^{-1} could be obtained.

A plausible reason for the relatively weak exchange interaction observed is given by the fact that the unpaired electron in $d_{x^2-y^2}$ orbital is localized in the basal plane of square pyramid and the orbital is pointing toward the four nearest neighbors of Cu(II) ion (N, N, O and X ions), as could be seen in Figure 3. Therefore, the two orbitals with unpaired electrons are situated in parallel planes, separated by ~ 3.5 Å, a particularly unfavorable arrangement for strong exchange interaction to occur.[41]
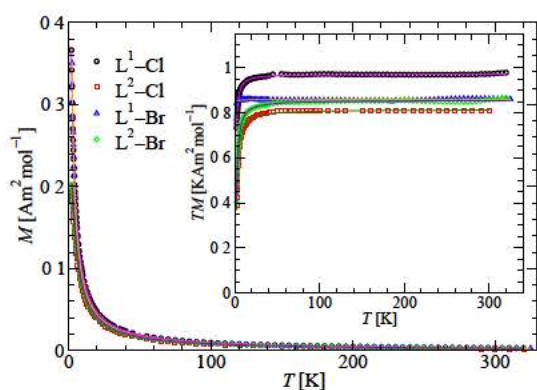
Fig. 7 Temperature dependence of magnetization, measured in field of 0.1 T. Inset: temperature dependence of $T \cdot M$ product. Lines are fitting curves.
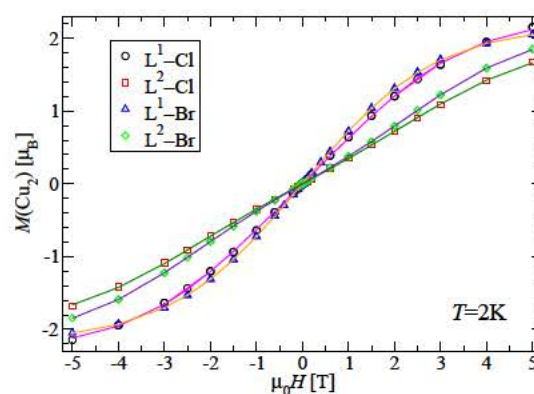

Fig. 8 Field dependence of magnetization. Lines are fitting curves.

Table 4 Exchange interaction parameters J and g-factors obtained from magnetization study

Compound	from $M(T)$		from $M(H)$	
	J(cm^{-1})	g	J(cm^{-1})	g
L^1–Cl	−0.59(1)	2.274(4)	−0.64(1)	2.283(4)
L^2–Cl	−1.19(3)	2.06(2)	−1.10(4)	2.00(2)
L^1–Br	−0.07(3)	2.149(9)	−0.13(3)	2.17(9)
L^2–Br	−1.18(1)	2.140(3)	−1.18(1)	2.167(3)

3.3 Magnetization study

Temperature dependence of magnetization $M(T)$ of the investigated complexes is presented in Figure 7. The observed magnetization, lower than expected for two independent copper(II) spins at low temperature, indicates antiferromagnetic interaction between spins in structural dimers for all four complexes. The interaction is weak, as could be clearly seen by looking at the inset of Figure 7, where the product $M \cdot T(T)$ curve is shown. It deviates from horizontal (paramagnetic) line below few Kelvins only and therefore the molar magnetic susceptibility can not be modelled using Bleaney-Bowers expression for interacting spins in dimers. Instead, since J is comparable to $g\beta H$, more general approach, developed by Friedberg, should be used[42,43]:

$$M = \frac{Ng\beta \sinh(g\beta H/kT)}{exp(|-2J|/kT) + 2\cosh(g\beta H/kT) + 1},\quad (4)$$

N, β and k are the well known constants, H is applied field, variable T is temperature, g is effective g-factor and J is isotropic exchange interaction parameter within dimer, defined through energy term $-2JS_1 \cdot S_2$. Besides the g and J fitting parameters, small correction to temperature independent core electron contribution is added. Fits of eq 4 go very well through the measured magnetization points, as could be seen in Figure 7. The fitting was performed in both $M(T)$ and $T \cdot M(T)$ forms giving approximately the same results. The obtained values are presented in Table 4 and standard deviation is included together with fitting error in parentheses.

The field dependence of magnetization $M(H)$ measured at temperature 2 K is presented in Figure 8. An advantage of Friedberg approach is the description of $M(H)$ curves up to arbitrary field H at every temperature T. The results of fitting the eq 4 to the $M(H)$ data are presented also in Table 4.

The exchange parameters J obtained from fitting $M(T)$ and

$M(H)$ curves are mutually similar and they are also in agreement with values obtained from EPR spectra, thus confirming the consistency of two experimental methods. Small discrepancies between the obtained g-factors and the average EPR values given in Table 3 could derive from the uncertainty of absolute magnetization due to sample mass measurements. Additionally, the high degree purity of the samples is confirmed through this analysis. Hence, from a magnetic point of view, the compounds can be considered as isolated halo-bridged copper(II) dimers. This result is in agreement with previously crystallographically described, infinite chain of dimeric units linked by H-bond via oxalamide groups. Due to the large size of the ligands, it can be seen that no magnetic interaction can take place through the organic bridge between dimers.

3.4 Magneto-structural correlation

Relationship between structural and magnetic properties in copper(II) dimer complexes has been intensively studied since 1970. It has been shown that exchange interaction is affected by several structural parameters such as the identity of the bridging atoms (X), the Cu–Cu' distances, the bridging angles Cu–X–Cu' (α), the dihedral angles containing Cu ions and the coordination geometries around copper ions.[5,9,44–48]

For planar dihydroxo-bridged copper complexes, a simple, linear, correlation between the singlet-triplet separation $2J$ and the angle α was reported.[44–46] However, in the case of dihalo-bridged copper complexes, the wider variety of geometries available to such systems and the possibility for relatively low-lying halogens' d-orbitals to interact with copper orbitals make the overall picture more complicated.[49] Generally, a strong correlation (parabolic curve with a maximum of ca. $33°/\text{Å}$) has been found between $2J$ and the quotient α/R, where R is the longer (axial) Cu–Cl distance.[50] It is pointed out that for the values $31 < \alpha/R < 34.5$, the exchange interaction is ferromagnetic and for the values $\alpha/R < 31$ or $\alpha/R > 34.5$ the exchange interaction is antiferromagnetic.[50] This is in agreement with the fact that $|J|$, always composed from ferro- and antiferromagnetic components should have minimal value.[43,46] Ferromagnetic contributions are usually small but antiferromagnetic contributions are proportional to the square of the overlap integral between orbitals. Therefore, the resulting sign depends on the amplitude of that overlap.[51] The above correlation rule is valid only for complexes with square-pyramidal arrangement of type II (pyramids share one base-to-apex edge with parallel basal planes)[28].

For complexes of type III (pyramids sharing a basal edge with coplanar basal planes), a linear dependence in the $2J$ vs. α/R graph is found. In other words, magneto-structural correlations of dichloro-bridged copper(II) complexes must take into account the relative orientation of square pyramids to each other, viz. coplanar, parallel and perpendicular. This is also in accordance with molecular orbitals calculations that indicate different type of orbitals involved in each case.[5] In this work, the experimental values $2J = -1.2\ \text{cm}^{-1}$ (with $\alpha/R = 32.9°/\text{Å}$) and $2J = -2.4\ \text{cm}^{-1}$ (with $\alpha/R = 34.3°/\text{Å}$) determined for dichloro-bridged complexes $\mathbf{L^1}$–Cl and $\mathbf{L^2}$–Cl respectively, are in contrast with the correlation rule for type II compounds previously described[50] and add to other similar cases of inconsistency[52]. However, the obtained results are quantitatively in agreement with other type II values, where the exchange interaction within dimer is generally $-10\ \text{cm}^{-1} < J < 10\ \text{cm}^{-1}$.[4]

For dibromo-bridged copper dimers, the situation is even more complicated. There is less information available for complexes bridged by Br compared to Cl and magneto-structural correlations are less studied for Br-bridged copper dimers.[10] It has been found that the previously mentioned correlation $2J$ vs. α/R ratio is not valid for dibromo-bridged copper complexes.[8,11] However, Landee and Greeney observed that the magnetic interaction strength can be correlated to the degree of non-planarity within the Cu basal plane (J vs. trans Br-Cu-L bridging angle)[8]. Similar correlation was presented by Rojo and coworkers which associated J to the extent of distortion within Cu basal plane and to the Cu–Br (apical) distance, including also different types of geometry such as reg-
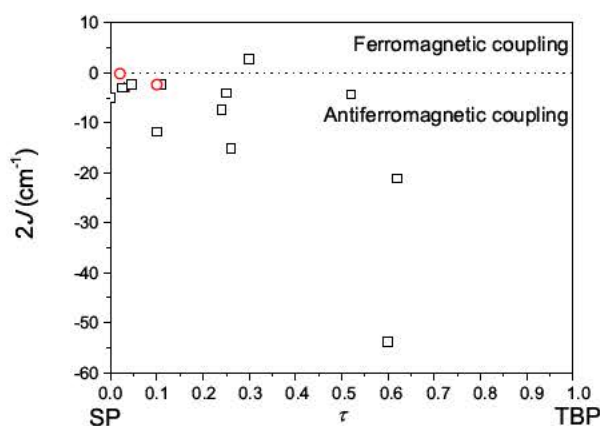

Fig. 9 Magneto-structural correlations for dibromo-bridged copper(II) complexes: plot of the singlet-triplet splitting $2J$ (cm^{-1}) vs. Reedijk's trigonal distortion parameter τ. Black squares present literature data given in Table 8 in SI, while red circles present values obtained for $\mathbf{L^1}$–Br and $\mathbf{L^2}$–Br complexes in this work. SP = square pyramid; TBP = trigonal bipyramid.

ular square pyramids, trigonal distorted square pyramids and tetrahedral distorted square pyramids.[48] Additionally, Romero and coworkers found a difference between two groups of dibromo-bridged copper complexes following Rodríguez classification.[28,53]

Here, a simple correlation between singlet-triplet splitting $2J$ and Reedijk's parameter τ of trigonal distortion is presented. The selected structural and magnetic data for complexes reported in literature[54–60] are shown in Table 8 in SI, while the related graph $2J$ vs. parameter τ is shown in Figure 9.

It should be noted that trigonal bipyramid could be considered as the limit case of distortion of square pyramid via the Berry mechanism.[53] It could be seen that only one complex is ferromagnetically coupled while the most complexes are weakly antiferromagnetically coupled with $|J| < 10\ \text{cm}^{-1}$, including the bromide complexes of this work. This is in agreement with Kahn's observation that 95% of copper(II) dinuclear compounds have antiferromagnetic interaction.[2] The strongest couplings are shown by trigonal bypiramid complexes. The observed behavior is relatively easy to be explained. For example, for type II complexes, the exchange pathway takes place through an interaction between copper $d_{x^2-y^2}$ situated in basal plane and the apical p bromo-orbital. Therefore, for small τ values, the density of magnetic orbital out of the plane is small and superexchange coupling would be weak or slightly ferromagnetic, while for an ideal square-pyramid geometry ($\tau = 0$), zero coupling is expected.

For distorted geometry around copper ion, magnetic orbitals are more mixed with bromo orbital and exchange interaction would be stronger. For trigonal-bypiramid geometry ($\tau = 1$), magnetic orbitals are on d_{z^2} and the overlap would again be zero.[10] The lack of dibromo-bridged copper complexes featuring geometries within $\tau = 0.65 - 1$ range prevents to verify such anticipated tendency. Finally, the hypothesis that bromide dimers might have stronger antiferromagnetic couplings than the chloride analogues[10,48,61] is not supported by our data as well as by those of others.[8]

4   Conclusions

In summary, we have designed and synthesized a set of four dihalo-bridged copper(II) dimers making use of oxalyl retropeptide ligands. Single-crystal X-ray diffraction analysis reveals that, in all cases, the Cu(II) ion is penta-coordinated by a tridentate NNO ligand and by two halo-ions (Cl or Br) in an ideal or near ideal square-pyramidal environment with $\tau = 0.00 - 0.17$. Single crystal EPR and SQUID magnetization studies on the dinuclear complexes confirm the presence of weak antiferromagnetic interactions between the copper ions. By considering the data available in the literature for similar dihalo-bridged copper(II) complexes, it appears evident that more studies and data analyzes are required in order to obtain better and more widely applicable magneto-structural correlations, especially for the less common Br-derivatives. Finally, the one-dimensional hydrogen bonded polynuclear arrangements observed in the solid state, suggest the potential application of such ligands as building blocks for the self-assembly of molecule-based magnetic materials. Work along these lines is in progress and will be reported in due course.

References

1. (a) I. A. Koval, P. Gamez, C. Belle, K. Selmeczi and J. Reedijk, *Chem. Soc. Rev.*, 2006, **35**, 814–840; (b) S. Tardito, I. Bassanetti, C. Bignardi, L. Elviri, M. Tegoni, C. Mucchino, O. Bussolati, R. Franchi-Gazzola and L. Marchiò, *J. Am. Chem. Soc.*, 2011, **133**, 6235–6242; (c) P. Hirva, A. Nielsen, A. D. Bond and C. J. McKenzie, *J. Phys. Chem. B*, 2010, **114**, 11942–11948.
2. O. Kahn, *Molecular Magnetism*, Wiley-VCH Inc., 1993.
3. (a) O. Kahn, Y. Pei and Y. Journaux, *Inorganic Materials*, John Wiley and Sons: Chichester, U.K., 1992; (b) O. Kahn, *Acc. Chem. Res.*, 2000, **33**, 647–657; (c) E. Pardo, J. Faus, M. Julve, F. Lloret, M. C. Muñoz, J. Cano, X. Ottenwaelder, Y. Journaux, R. Carrasco, G. Blay, I. Fernández and R. Ruiz-García, *J. Am. Chem. Soc.*, 2003, **125**, 10770–10771.
4. A. Rodríguez-Fortea, P. Alemany, S. Alvarez and E. Ruiz, *Inorg. Chem.*, 2002, **41**, 3769–3778.
5. M. Rodríguez, A. Llobet and M. Corbella, *Polyhedron*, 2000, **19**, 2483–2491.
6. B. Murphy and B. Hathaway, *Coord. Chem. Rev.*, 2003, **243**, 237–262.
7. (a) A. Sasmal, S. Shit, C. Rizzoli, H. Wang, C. Desplanches and S. Mitra, *Inorg. Chem.*, 2012, **51**, 10148–10157; (b) K. Skorda, T. C. Stamatatos,

A. P. Vafiadis, A. T. Lithoxoidou, A. Terzis, S. P. Perlepes, J. Mrozinski, C. P. Raptopoulou, J. C. Plakatouras and E. G. Bakalbassis, *Inorg. Chim. Acta*, 2005, **358**, 565–582.
8. C. P. Landee and R. E. Greeney, *Inorg. Chem.*, 1986, **25**, 3771–3775.
9. T. Rojo, M. I. Arriortua, J. Ruiz, J. Darriet, G. Villeneuve and D. Beltran-Porter, *J. Chem. Soc., Dalton Trans.*, 1987, 285–291.
10. S. Sain, T. K. Maji, D. Das, J. Cheng, T.-H Lu, J. Ribas, M. S. El Fallah and N. R. Chaudhuri, *J. Chem. Soc., Dalton Trans.*, 2002, 1302–1306.
11. D. K. Towle, S. K. Hoffmann, W. E. Hatfield, P. Singh, P. Chaudhuri and K. Wieghardt, *Inorg. Chem.*, 1985, **24**, 4393–4397.
12. (a) M.-C. Dul, E. Pardo, R. Lescouëzec, Y. Journaux, J. Ferrando-Soria, R. Ruiz-García, J. Cano, M. Julve, F. Lloret, D. Cangussu, C. L. Pereira, H. O. Stumpf, J. Pasán and C. Ruiz-Pérez, *Coord. Chem. Rev.*, 2010, **254**, 2281–2296; (b) R. Ruiz, J. Faus, F. Lloret, M. Julve and Y. Journaux, *Coord. Chem. Rev.*, 1999, **193-195**, 1069–1117.
13. Z. Džolić, M. Cametti, D. Milić and M. Žinić, *Chem.-Eur. J.*, 2013, **19**, 5411–5416.
14. Agilent, *CrysAlis PRO*, Agilent Technologies UK Ltd: Yarnton, U. K., 2011.
15. G. M. Sheldrick, *Acta Crystallogr., Sect. A*, 2008, **64**, 112–122.
16. P. Emsley, B. Lohkamp, W. G. Scott and K. Cowtan, *Acta Crystallogr. Sect. D*, 2010, **66**, 486–501.
17. L. J. Farrugia, *J. Appl. Crystallogr.*, 1999, **32**, 837–838.
18. A. L. Spek, *Acta Crystallogr., Sect. D*, 2009, **65**, 148–155.
19. C. F. Macrae, I. J. Bruno, J. A. Chisholm, P. R. Edgington, P. McCabe, E. Pidcock, L. Rodriguez-Monge, R. Taylor, J. Van De Streek and P. A. Wood, *J. Appl. Crystallogr.*, 2008, **41**, 466–470.
20. L. J. Farrugia, *J. Appl. Cryst.*, 1997, **30**, 565.
21. *Persistence of Vision Pty. Ltd., Persistence of Vision Raytracer (POV-Ray; Version 3.6). http://www.povray.org/*, 2004.
22. (a) L. Frkanec and M. Žinić, *Chem. Commun.*, 2010, **46**, 522–537; (b) Z. Džolić, M. Cametti, A. Dalla Cort, L. Mandolini and M. Žinić, *Chem. Commun.*, 2007, 3535–3537; (c) A. Guerrero-Martínez, B. Auguié, J. L. Alonso-Gómez, Z. Džolić, S. Gómez-Graña, M. Žinić, M. M. Cid and L. M. Liz-Marzán, *Angew. Chem. Int. Ed.*, 2011, **50**, 5499–5503; (d) G. De Paoli, Z. Džolić, F. Rizzo, L. De Cola, F. Vögtle, W. Müller, G. Richardt and M. Žinić, *Adv. Funct. Mater.*, 2007, **17**, 821–828; (e) Z. Džolić, K. Wolsperger and M. Žinić, *New J. Chem.*, 2006, **30**, 1411–1419.
23. A. Cornia, A. C. Fabretti, F. Ferraro, D. Gatteschi and A. Giusti, *J. Chem. Soc., Dalton Trans.*, 1993, 3363–3366.
24. J.-K. Tang, Y. Ou-Yang, H.-B. Zhou, Y.-Z. Li, D.-Z. Liao, Z.-H. Jiang, S.-P. Yan and P. Cheng, *Cryst. Growth Des.*, 2005, **5**, 813–819.
25. L. Shi, B. Cai, G. Huang, J.-Z. Wu and Y. Yu, *Anorg. Allg. Chem.*, 2011, **637**, 306–311.
26. (a) F. Lloret, M. Julve, J. Faus, Y. Journaux, M. Philoche-Levisalles and Y. Jeannin, *Inorg. Chem.*, 1989, **28**, 3702–3706; (b) H.-X. Zhang, B.-S. Kang, Z.-Y. Zhou, A. S. C. Chan, Z.-N. Chen and C. Ren, *J. Chem. Soc., Dalton Trans.*, 2001, 1664–1669; (c) L.-H. Xu, H.-X. Wang and L.-N. Zhu, *J. Coord. Chem.*, 2012, **65**, 1051–1061.
27. A. W. Addison, T. N. Rao, J. Reedijk, J. van Rijn and G. C. Verschoor, *J. Chem. Soc., Dalton Trans.*, 1984, 1349–1356.
28. M. Rodríguez, A. Llobet, M. Corbella, A. E. Martell and J. Reibenspies, *Inorg. Chem.*, 1999, **38**, 2328–2334.
29. (a) D. W. Phelps, W. H. Goodman and D. J. Hodgson, *Inorg. Chem.*, 1976, **15**, 2266–2270; (b) M. Melník, M. Kabešová, M. Koman, Ľ. Macášková, J. Garaj, C. E. Holloway and A. Valent, *J. Coord. Chem.*, 1998, **45**, 147–359; (c) B. Antonioli, B. Buchner, J. K. Clegg, K. Gloe, K. Gloe, L. Gotzke, A. Heine, A. Jager, K. A. Jolliffe, O. Kataeva, V. Kataev, R. Klingeler, T. Krause, L. F. Lindoy, A. Popa, W. Seichter and M. Wenzel, *Dalton Trans.*, 2009, 4795–4805; (d) C. P. Pradeep and S. K. Das, *Polyhedron*, 2009, **28**, 630–636.
30. S. J. Brown, X. Tao, T. A. Wark, D. W. Stephan and P. K. Mascharak,

Inorg. Chem., 1988, **27**, 1581–1587.

31 (*a*) A. Castiñeiras, A. G. Sicilia-Zafra, J. M. González-Pérez, D. Choquesillo-Lazarte and J. Niclós-Gutiérrez, *Inorg. Chem.*, 2002, **41**, 6956–6958; (*b*) Z. D. Tomić, V. M. Leovac, S. V. Pokorni, D. Zobel and S. D. Zarić, *Eur. J. Inorg. Chem.*, 2003, **2003**, 1222–1226; (*c*) Z. D. Tomić, S. B. Novaković and S. D. Zarić, *Eur. J. Inorg. Chem.*, 2004, **2004**, 2215–2218; (*d*) Z. D. Tomić, D. Sredojević and S. D. Zarić, *Cryst. Growth Des.*, 2006, **6**, 29–31.

32 (*a*) G. A. Bogdanović, A. S.-d. Biré and S. D. Zarić, *Eur. J. Inorg. Chem.*, 2002, **2002**, 1599–1602; (*b*) Y.-f. Jiang, C.-j. Xi, Y.-z. Liu, J. Niclós-Gutiérrez and D. Choquesillo-Lazarte, *Eur. J. Inorg. Chem.*, 2005, **2005**, 1585–1588; (*c*) D. Sredojević, G. A. Bogdanović, Z. D. Tomić and S. D. Zarić, *CrystEngComm*, 2007, **9**, 793–798; (*d*) V. B. Medaković, G. A. Bogdanović, M. K. Milčić, G. V. Janjić and S. D. Zarić, *J. Inorg. Biochem.*, 2012, **117**, 157–163.

33 H. Yokoi and S. Ohsawa, *Bull. Chem. Soc. Jpn.*, 1973, **46**, 2766–2768.

34 J. A. Weil, J. R. Bolton and J. E. Wertz, *Electron Paramagnetic Resonance*, John Wiley and Sons, Inc., New York, 1994.

35 E. Garribba and G. Micera, *J. Chem. Educ.*, 2006, **83**, 1229.

36 S. Stoll and A. Schweiger, *J. Magn. Reson.*, 2006, **178**, 42–55.

37 L. J. De Jongh, *Magnetic Properties of Layered Transition Metal Compounds*, Kluwer Academic Publishers, The Netherlands, 1990.

38 (*a*) R. Calvo, *Appl. Magn. Reson.*, 2007, **31**, 271–299; (*b*) P. Levstein, C. Steren, A. Gennaro and R. Calvo, *Chem. Phys.*, 1988, **120**, 449–459; (*c*) A. Gennaro, P. Levstein, C. Steren and R. Calvo, *Chem. Phys.*, 1987, **111**, 431–438; (*d*) R. D. Willett, F. H. Jardine, I. Rouse, R. J. Wong, C. P. Landee and M. Numata, *Phys. Rev. B*, 1981, **24**, 5372–5381.

39 (*a*) J. E. Wertz and J. R. Bolton, *Electron Spin Resonances, Elementary Theory and Practical Applications*, McGraw-Hill, New York, 1972; (*b*) C. P. Poole, Jr., *Electron Spin Resonance: A Comprehensive Treatise on Experimental Techniques*, John Wiley and Sons, Inc., New York, 1983.

40 L. Androš, M. Jurić, P. Planinić, D. Žilić, B. Rakvin and K. Molčanov, *Polyhedron*, 2010, **29**, 1291–1298.

41 I. Bkouche-Waksman, S. Sikorav and O. Kahn, *J. Cryst. Spec. Res.*, 1983, **13**, 303–310.

42 B. E. Myers, L. Berger and S. A. Friedberg, *J. Appl. Phys.*, 1969, **40**, 1149–1151.

43 C. R. Lucas, S. Liu and L. K. Thompson, *Inorg. Chem.*, 1990, **29**, 85–88.

44 V. H. Crawford, H. W. Richardson, J. R. Wasson, D. J. Hodgson and W. E. Hatfield, *Inorg. Chem.*, 1976, **15**, 2107–2110.

45 D. Y. Jeter, D. L. Lewis, J. C. Hempel, D. J. Hodgson and W. E. Hatfield, *Inorg. Chem.*, 1972, **11**, 1958–1960.

46 P. J. Hay, J. C. Thibeault and R. Hoffmann, *J. Am. Chem. Soc.*, 1975, **97**, 4884–4899.

47 K. Das, A. Datta, C. Sinha, J.-H. Huang, E. Garribba, C.-S. Hsiao and C.-L. Hsu, *ChemistryOpen*, 2012, **1**, 80–89.

48 T. Rojo, M. I. Arriortua, J. L. Mesa, R. Cortes, G. Villeneuve and D. Beltran, *Inorg. Chim. Acta*, 1987, **134**, 59–66.

49 W. E. Marsh, T. L. Bowman, C. S. Harris, W. E. Hatfield and D. J. Hodgson, *Inorg. Chem.*, 1981, **20**, 3864–3867.

50 W. E. Marsh, K. C. Patel, W. E. Hatfield and D. J. Hodgson, *Inorg. Chem.*, 1983, **22**, 511–515.

51 E. Colacio, M. Ghazi, R. Kivekäs and J. M. Moreno, *Inorg. Chem.*, 2000, **39**, 2882–2890.

52 X.-H. Jin, L.-X. Cai, J.-K. Sun, Z.-F. Ju and J. Zhang, *Inorg. Chem. Commun.*, 2010, **13**, 86 – 89.

53 M. Romero, J. Salas, M. Quirós, M. P. Sánchez, J. Romero and D. Mart´in, *Inorg. Chem.*, 1994, **33**, 5477–5481.

54 P. Singh, D. Y. Jeter, W. E. Hatfield and D. J. Hodgson, *Inorg. Chem.*, 1972, **11**, 1657–1661.

55 M. Megnamisi-Belombe and M. A. Novotny, *Inorg. Chem.*, 1980, **19**, 2470–2473.

56 W. E. Marsh, T. L. Bowman, W. E. Hatfield and D. J. Hodgson, *Inorg.*

Chim. Acta, 1982, **59**, 19–24.

57 R. Li, B. Moubaraki, K. S. Murray and S. Brooker, *Dalton Trans.*, 2008, 6014–6022.

58 E. Luukkone and A. Pajunen, *Suom. Kemistil. B*, 1973, **46**, 292–296.

59 R. B. Wilson, W. E. Hatfield and D. J. Hodgson, *Inorg. Chem.*, 1976, **15**, 1712–1716.

60 J. T. Blanchette and R. D. Willett, *Inorg. Chem.*, 1988, **27**, 843–849.

61 W. E. Estes, J. R. Wasson, J. W. Hall and W. E. Hatfield, *Inorg. Chem.*, 1978, **17**, 3657–3664.

4.1 Acknowledgement

5 Supplementary Information

Table 5 Hydrogen-bonding parameters (Å, °) in crystal structures of the studied complexes

	D–H$\cdots$A	D–H	H$\cdots$A	D$\cdots$A	D–H$\cdots$A	Symmetry operator on A
L^1–Cl	N3–H3N$\cdots$O5	0.86(2)	2.08(3)	2.858(3)	150(2)	$1+x, 1+y, z$
	N6–H6N$\cdots$O1	0.85(2)	1.99(3)	2.816(3)	163(2)	$-1+x, -1+y, z$
	O9–H9A$\cdots$Cl2	0.84	2.46	3.256(5)	158	.
	C2–H2$\cdots$O9	0.95	2.42	3.240(7)	144	$1+x, y, z$
	C19–H19$\cdots$O3	0.95	2.46	3.126(4)	127	$-1+x, y, z$
	C20–H20$\cdots$Cl2	0.95	2.79	3.366(2)	120	.
	C25–H25A$\cdots$O1	0.99	2.54	3.257(3)	129	$-1+x, -1+y, z$
L^2–Cl	N3–H3N$\cdots$O1	0.86(2)	1.96(2)	2.721(3)	147(2)	$1-x, 1-y, 1-z$
	C15A–H15A$\cdots$O2	0.95	2.50	3.183(5)	129	.
L^1–Br	N3–H3N$\cdots$O5	0.88	1.96	2.796(5)	159	$1+x, y, -1+z$
	N6–H6N$\cdots$O1	0.88	1.98	2.758(5)	146	$-1+x, y, 1+z$
	C3–H3$\cdots$O7	0.95	2.35	3.241(6)	157	$1+x, y, z$
	C10–H10B$\cdots$O5	0.99	2.46	3.101(5)	122	$1+x, y, -1+z$
L^2–Br	N3–H3N$\cdots$O1	0.88	2.09	2.802(6)	138	$2-x, 1-y, 1-z$

Table 6 Stacking interactions (Å, °) in the studied crystal structures

	Ring $m\cdots$Ring n^a	$Cgm\cdots Cgn^b$	α^c	Mean plane of Ring $m\cdots Cgn$	Ring offset	Symmetry n operator on ring
L^1–Cl	Ring 1$\cdots$Ring 4	3.644(1)	4.9(1)	3.528(1)		$1+x, y, z$
	Ring 2$\cdots$Ring 3	3.647(1)	8.1(1)	3.542(1)		$x-1, y, z$
L^1–Br	Ring 1$\cdots$Ring 4	3.675(2)	5.4(2)	3.482(2)		$1+x, y, z$
	Ring 2$\cdots$Ring 3	3.652(2)	6.8(2)	3.492(2)		$x-1, y, z$
L^2–Br	Ring 1$\cdots$Ring 3	3.601(3)	5.7(2)	3.496(2)		$2-x, 1-y, -z$
	Ring 5$\cdots$Ring 5	3.708(4)	0	3.566(3)	*cca* 1.02	$1-x, -y, 1-z$

^{a} Definition of the rings:
Ring 1 - metalloaromatic chelate ring Cu1/O2/C8/C7/N2;
Ring 2 - metalloaromatic chelate ring Cu2/O6/C23/C22/N5;
Ring 3 - pyridyl ring N1/C1–C5;
Ring 4 - pyridyl ring N4/C16–C20;
Ring 5 - phenyl ring C10–C15.
^{b} Cgm and Cgn are centroids of the rings m and n.
^{c} α is the dihedral angle between the mean planes of the two interacting rings (m and n).

Table 7 C–H$\cdots\pi$ interactions (Å, °) in the studied structures

	D–H$\cdots Cg^a$	H$\cdots Cg$	$D\cdots Cg$	D–H$\cdots Cg$	Symmetry operator on Cg
L^2–Cl	C2–H2$\cdots Cg$5A	2.68	3.573(4)	156	$-x, 1-y, 1-z$
	C2–H2$\cdots Cg$5B	2.82	3.527(7)	132	$-x, 1-y, 1-z$
	C6–H6$\cdots Cg$1	3.00	3.927(2)	157	$-x, 1-y, 1-z$
L^1–Br	C28–H28C$\cdots Cg$1	2.95	3.586(5)	123	$x, y, z+1$
L^2–Br	C3–H3$\cdots Cg$5	2.58	3.464(6)	154	$2-x, 1-y, -z$
	C13–H13$\cdots Cg$1	2.98	3.908(7)	167	$x, y-1, z$

^{a} Definition of the ring centroids:

Cg1 - metalloaromatic chelate ring Cu1/O2/C8/C7/N2;

Cg5 - phenyl ring C10A–C15A;

Cg5A - phenyl ring of **L^2–Cl** in the major disordered conformation C10A–C15A;

Cg5B - phenyl ring of **L^2–Cl** in the minor disordered conformation C10B–C15B.
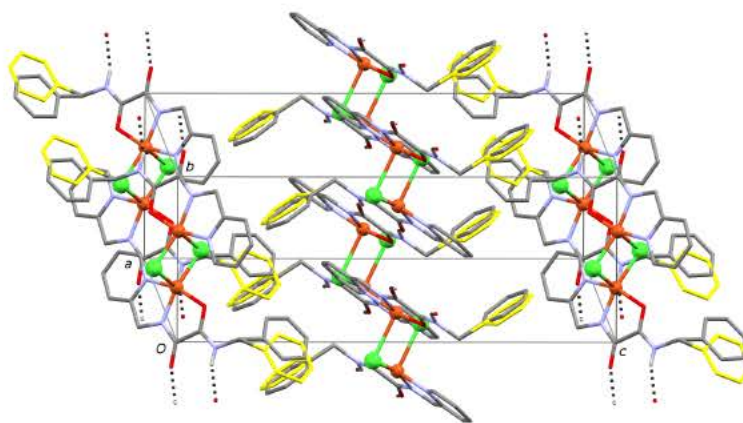
Fig. 10 Molecular packing in the crystal structure of **L^2–Cl**. Cu and Cl atoms are shown as spheres. Minor conformation of the disordered *N*-benzyl group is depicted in yellow. Hydrogen bonds between oxalamide units are represented as dotted lines. H atoms bound to C atoms are omitted for clarity.
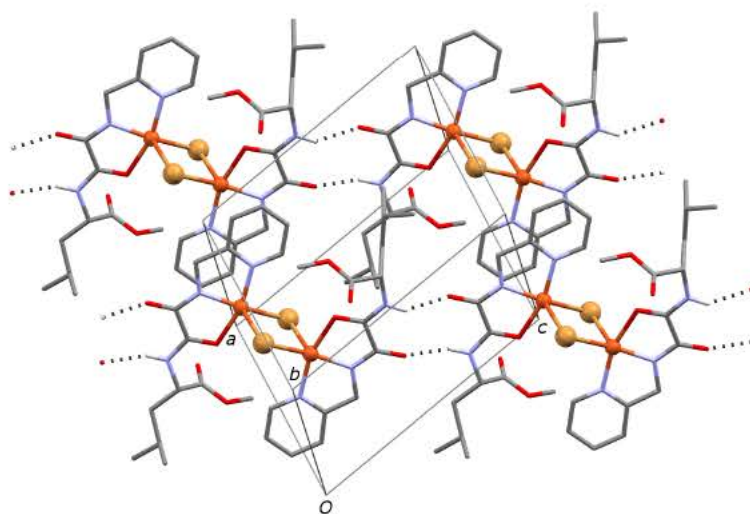
Fig. 11 Molecular packing in the crystal structure of L^1–**Br**. Cu and Br atoms are shown as spheres. Hydrogen bonds between oxalamide units are represented as dotted lines. H atoms attached to C atoms are omitted for clarity.
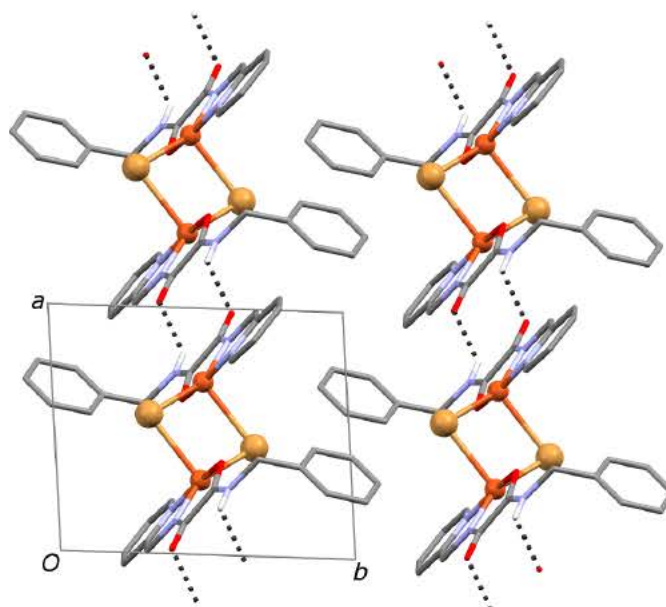

Fig. 12 Molecular packing in the crystal structure of L^2–**Br** viewed along the crystallographic c axis. Cu and Br atoms are shown as spheres. Hydrogen bonds between oxalamide units are represented as dotted lines. H atoms bound to C atoms are omitted for clarity.

Table 8 Structural and magnetic properties for the selected dibromo-bridged copper(II) dimers

Compound[a]	Geometry	τ	$2J(\text{cm}^{-1})$	Ref.
$[Cu(\alpha\text{-pic})_2Br_2]_2$	SP	0	-5	54
$[Cu(dmen)Br_2]_2$	SP	0.11	-2.4	29
$[Cu(dmgH)Br_2]_2$	SP	0.025	-3.02	55
$[Cu(4\text{-metz})_2Br_2]_2$	SP	0.045	-2.4	49
$[Cu(dien)Br_2]_2(ClO_4)_2$	SP	0.3	2.8	11
$[Cu(4\text{-meox})_2Br_2]_2$	SP	0.26	-15.2	56
$[Cu(terpy)Br]_2(PF_6)_2$	SP	0.24	-7.4	48
$[Cu(L^a)Br_2]_2$	SP	0.02;0.1	-11.76	10
$[Cu(L^b)Br]_2$	SP	0.03	-3.14	57
$[Cu(tmen)Br_2]_2$	SP	0.25	-4	53,58
L^1–Br	SP	0.04;0.00	-0.14	this work
L^2–Br	SP	0.10	-2.36	this work
$[Cu(MAEP)Br_2]_2$	TBP	0.52	-4.3	59
$(3ap)_2[Cu_2Br_6]_2 \cdot 2H_2O$	TBP	0.6	-53.8	60
$[Cu(dmtp)_2Br_2]_2 \cdot 2H_2O$	TBP	0.62	-21.1	53

[a] Abbreviations: α-pic = α-picoline (2-methylpyridine); MAEP = 2-(2-(methylamino)ethyl)pyridine; dmen = *N,N*-dimethylethylenediamine; dmgH = dimethylglyoxime; 4-metz = 4-methylthiazole; dien = diethylenetriamine; 4-meox = 4-methyloxazole; terpy = 2,2':6',2''-terpyridine; L^a = 1,4-diazacycloheptane; HL^b = *N*-(1H-pyrrol-2-ylmethylene)-2-pyridineethanamine; tmen = *N,N,N',N'*-tetramethylethylenediamine; 3ap = 3-aminopyridinium cation; dmtp = 5,7 dimethyl-1,2,4-triazolo[1,5-α]pyrimidine; SP = square pyramid and TBP = trigonal bipyramid.
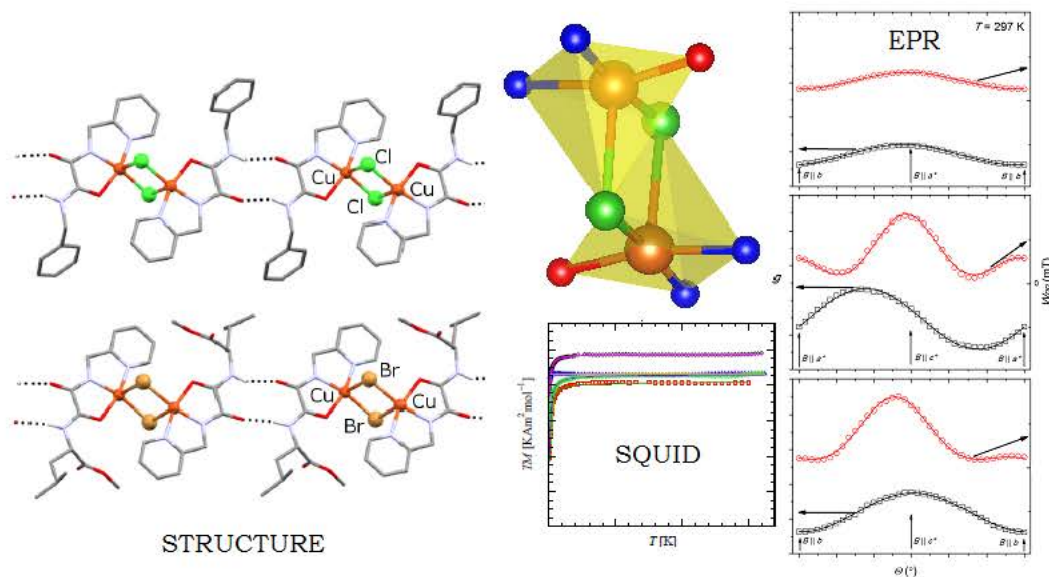

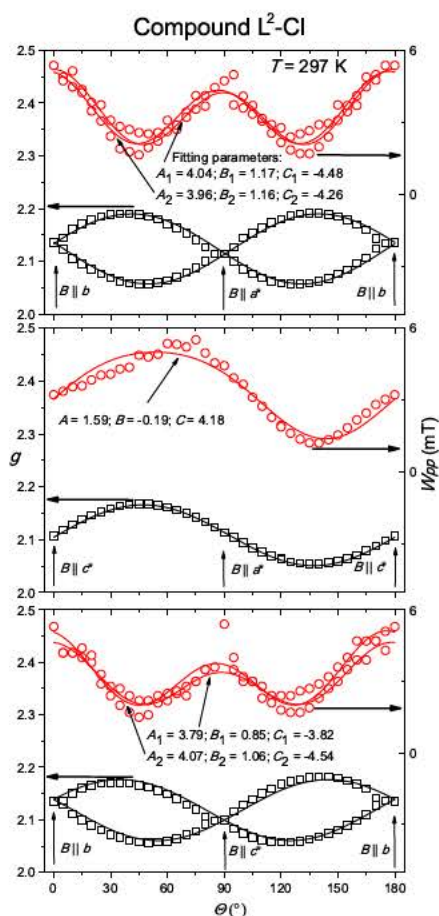**Fig. 16** For Table of Contents Only/AbstractGraphics

Fig. 13 Angular variation of the g-values (black squares) and the W_{pp} linewidths (red circles) of EPR lines for the single crystal of compound $\mathbf{L^2}$–**Cl**, at room temperature, in three mutually perpendicular planes. Solid lines represent the fitted g-values with parameters given in Table 2 and W_{pp} linewidths with parameters given in the figure, according to eq 1 and eq 2, respectively.
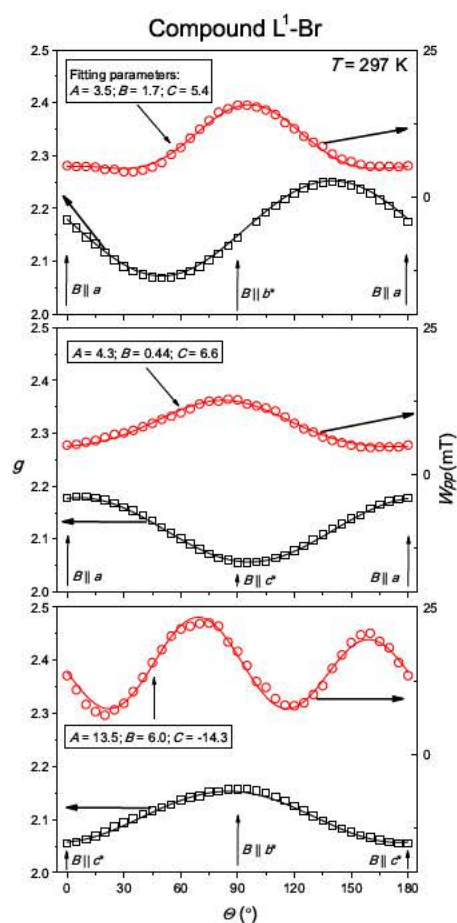
Fig. 14 Angular variation of the g-values (black squares) and the W_{pp} linewidths (red circles) of EPR lines for the single crystal of compound $\mathbf{L^1}$–**Br**, at room temperature, in three mutually perpendicular planes. Solid lines represent the fitted g-values with parameters given in Table 2 and W_{pp} linewidths with parameters given in the figure, according to eq 1 and eq 2, respectively.
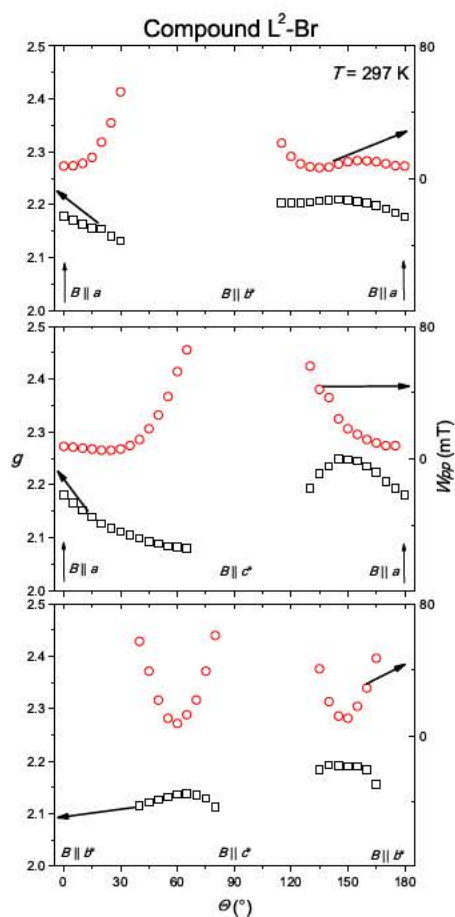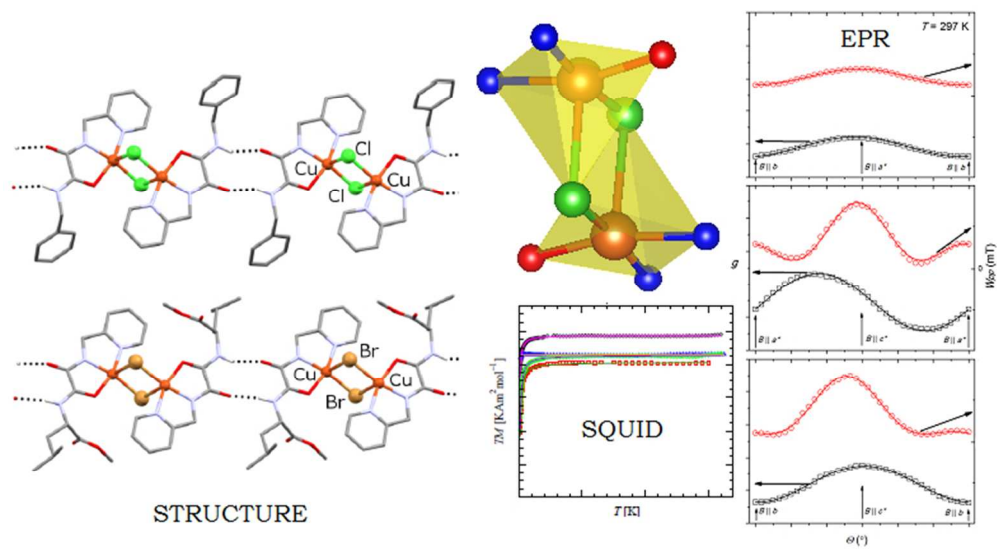
Fig. 15 Angular variation of the g-values (black squares) and the W_{pp} linewidths (red circles) of EPR lines for the single crystal of compound L^2–Br, at room temperature, in three mutually perpendicular planes. Some EPR lines were to weak and/or to broad to be detected.

208x116mm (96 x 96 DPI)